JOURNAL OF PROPULSION AND POWER
Vol. 24, No. 2, March–April 2008

Liquid-Fueled Strut-Based Scramjet Combustor Design: A Computational Fluid Dynamics Approach

P. Manna, Ramesh Behera, and Debasis Chakraborty*
Defence Research and Development Laboratory, Hyderabad 500 058, India

DOI: 10.2514/1.28333

Computational-fluid-dynamics-based design and analysis is presented for a full-scale scramjet combustor with kerosene fuel injected from struts placed in the combustor flowpath. Three-dimensional Navier–Stokes equations are solved with a *K-ε* turbulence model using commercial computational-fluid-dynamics software. Combustion is modeled based on infinitely fast chemical kinetics. Lagrangian dispersed-phase analysis is considered for fuel-droplet evaporation and mixing in the supersonic stream. Parametric studies are carried out to investigate the effect of combustor-inlet Mach number and total pressure on the flow development process. A higher combustor-entry Mach number and distributed-fuel-injection system will ensure the existence of predominant supersonic flow in the combustor. Simulations are also carried out to investigate two different kinds of fuel injection struts in the scramjet combustor performance. A distributed-fuel-injection system, required to avoid thermal choking, increases the three-dimensionality of the flowfield.

Nomenclature

A	=	coefficient matrix
C_μ, $C_{\varepsilon 1}$, $C_{\varepsilon 2}$	=	turbulence model constants
H	=	enthalpy, the height of the combustor
h	=	cavity depth, heat transfer coefficient
h_c	=	convective heat transfer coefficient per unit area A_p
K	=	turbulent kinetic energy
L	=	length of the combustor, latent heat of vaporization of fuel
$L_v \delta m_v$	=	energy required to vaporize volatiles of mass δm_v
m	=	mass of particle
$\dot{N}$	=	number of particles injected per unit time along the path
P	=	pressure
Pr	=	Prandtl number
$Q_c \delta m_c$	=	energy generated in the burning char of mass δm_c
q	=	heat flux
R	=	residue, mixing rate of combustion model
S	=	Sutherland's constant
S_K, S_ε	=	source terms for K and ε
T	=	temperature
T_p, T_f	=	particle and fluid temperature
t	=	time
u	=	velocity
v_f, v_p	=	fluid and particle velocity
W	=	width of the combustor
x, y, z	=	coordinate axes
Y	=	mass fraction
Z	=	species mass fraction
δm_p	=	mass loss of a particle in time step δt
δt	=	time step over which sources are applied
ε	=	turbulent kinetic energy dissipation rate
λ	=	thermal conductivity
ρ, μ, d	=	density, viscosity, and diameter of a particle
σ_K, σ_ε, σ_c	=	coefficients for K, ε, and Z equations
τ	=	shear stress

Subscripts

f	=	fuel
i, j, k	=	axial direction
l	=	laminar
p	=	combustion products, particle
o	=	oxidizer, stagnation value
s	=	static value
t	=	turbulent
α	=	freestream value

I. Introduction

THE quest for efficient hypersonic airbreathing propulsion for civil and military applications has driven the development of the scramjet engine since the early 1960s [1,2]. Both hydrogen and kerosene were studied for the fuel of the scramjet engine. Although hydrogen has attractive features in terms of specific impulse, ignition characteristics, etc., liquid hydrocarbon is required for volume-limited applications in lower hypersonic regions ($M < 8$), in view of their higher volumetric energy content, lower cost, and relative simplicity of operational use. Hypersonic military applications are typically associated with liquid hydrocarbons and a maximum Mach number of 8. Atomization, vaporization, mixing, and slow chemical reactions are some of the major barriers in the realization of a liquid-hydrocarbon-based scramjet. A deeper penetration of fuel into a supersonic airstream is required for better mixing, which is a key to sustained combustion. The penetration of the liquid jet depends on dynamic pressure ratios of two streams and the droplet size [3]. For a practical scramjet combustor in the flight region of Mach 6–7, the typical penetration height of the fuel jet is about 10 to 15 mm. Experimental and numerical simulations [4,5] have shown that fuel injection from the combustor wall will result in reaction zones that occupy only a small fraction of the flowfield. Therefore, not all of the oxygen supplied by the airstream entering into the combustor can participate in the heat-release process. Furthermore, the reaction zone close to the wall will exert excessive thermal loads on the structure of the combustor. The problem of slow lateral fuel transport in the airstream can be circumvented by injecting the fuel in the core region of the flow by means of struts and/or pylons. The oblique shocks generated from the struts also augment the mixing, which is very much needed in high-speed propulsion devices.

Received 13 October 2006; accepted for publication 31 October 2007. Copyright © 2007 by the American Institute of Aeronautics and Astronautics, Inc. All rights reserved. Copies of this paper may be made for personal or internal use, on condition that the copier pay the $10.00 per-copy fee to the Copyright Clearance Center, Inc., 222 Rosewood Drive, Danvers, MA 01923; include the code 0748-4658/08 $10.00 in correspondence with the CCC.

*Directorate of Computational Dynamics; debasis_drdl@yahoo.co.in.

Fuel injection from the struts has been experimented with in some subscale scramjet engines, including the airframe-integrated scramjet module [6,7]. The subscale scramjet engine being developed [7] uses the fuel injection strut to improve mixing. Scramjet engines with struts were tested for Mach 4, 6, and 8 conditions [7–9]. A large number of experimental and numerical studies [10–17] were reported in the literature to focus on various aspects of flow phenomena such as drag losses, mixing, combustion, intake combustor interaction, etc., in strut-based scramjet combustors with hydrogen fuel. The reported experimental and numerical studies on kerosene-fueled supersonic combustion mostly address the issues of a cavity-based flame holder and injection system [18–24] in a laboratory-scale combustor. The penetration of fuel in supersonic flow is critical in any practical scramjet combustor. The studies on strut-based scramjet combustors with kerosene fuel are highly limited. Vinogradov et al. [25] conducted an experimental investigation to determine the ignition, piloting, and flame-holding characteristics in a scramjet combustor operating on kerosene. To improve the fuel distribution and mixing, kerosene was injected from the strut located in the middle of the duct. Stable combustion of kerosene was achieved even after turning off the pilot hydrogen. Bouchez et al. [26] carried out an experimental investigation of a hydrocarbon-fueled scramjet combustor. Two identical metallic water-cooled and liquid-kerosene-cooled struts were used for the fuel injection in the combustor. To ensure ignition, pilot flames with gaseous hydrogen were used at the base of the struts. The kerosene equivalence ratio was varied from 0 to 1.0. Various flow parameters (wall pressure, wall heat flux, total temperature at combustor exit, thrust, etc.) were measured. Optical methods such as passive spectroscopy were also used to characterize the flow. The experimental results were used to validate the computational fluid dynamics (CFD) codes for the prediction of kerosene-fueled scramjet combustor flowfield.

With the advent of powerful computers and robust numerical algorithms, CFD complements difficult-to-perform experiments and thus plays a major role in developing a comprehensive understanding of the key phenomena that dominate performances. To accurately model a scramjet flowfield, CFD must adequately resolve several complex physical processes, including three-dimensionality, shock–boundary interaction, turbulent mixing of high-speed streams, and atomization and combustion of liquid fuel. Only a very few numerical studies were reported on strut-based liquid-fueled scramjet combustors. Dufour and Bounchez [27] numerically simulated the scramjet experiment [26] using a three-dimensional Navier–Stokes solver and single-step chemical kinetics. A reasonably good match is obtained between the computational and experimentally measured wall static pressure. It proceeds from the results that the pressure recovery and combustion efficiency can be predicted confidently from the simulation. These computations also confirmed that for the specific injected design investigated, the combustion efficiency is limited by an imperfect mixing between fuel and air.

Behera and Chakraborty [28] numerically simulated the flow features of a ramp-cavity-based subscaled combustor with kerosene fuel using the commercial software CFX-TASCflow [29]. A very good comparison between the experimental and computational surface pressure forms the basis of the thermochemical exploration of the flowfield.

Panneerselvam et al. [30] presented a hypersonic-cruise airbreathing mission with an airframe-integrated scramjet engine. The design and performance parameters of various individual components such as forebody, intake, combustor, and nozzle were presented. A generalized steady quasi-one-dimensional flow model was adopted to analyze the flowfield in the combustor. The analysis did not take into account various injection systems and the resulting shocks in the engine flowpath. Because drag and thrust must match in an airbreathing cruise mission, it is necessary to predict the thrust in the combustor with all geometrical and flow complexities.

In this work, three-dimensional viscous simulations are presented for a half-module scramjet combustor for a hypersonic airbreathing mission [30] with kerosene fuel injected from a row of struts placed in the flowpath. Thermochemical parameters are analyzed to estimate the flow behavior in the combustor. Performances of the scramjet combustor are estimated with different injector locations and combustor-entry conditions.

II. Consideration for Simulation

A typical cruise hypersonic airbreathing mission is explained in [30]. Demonstration of the autonomous functioning of an airframe-integrated scramjet engine in cruise mode for 20 s is envisaged. The operating Mach number and altitudes are 6.5 and 32.5 km, respectively. The design of the scramjet engine for the mission is highly challenging. To support the cruise mission, the achieved thrust must be equal to the drag incurred by the vehicle.

Considering the limitation of the connected-pipe-mode test facility, development of the scramjet combustor was focused to the half-module. To understand the complex flow features in the combustor and to obtain required thrust for the mission, various numerical simulations were performed for the half-module combustor with different sizes of the combustor, combustor-entry Mach number ,and total pressure, injection location, etc., while maintaining the same mass flow rate, total temperature, equivalence ratio, and total number of strut. The rationale behind these selections is as follows: Because operating altitude and freestream Mach number are defined, the total temperature is fixed. Because the capture mass flow rate is a strong function of the forebody design and the width of the intake, no variation of mass flow rate is considered. Because the flow compression inside the intake can be altered with change of the centerbody and the cowl surfaces, a different total pressure and combustor-entry Mach number can be achieved. The width of the combustor is kept constant. The length and the height of the combustor are varied while ascertaining if the combustor can be fitted in the overall vehicle envelope without much drag penalty.

The schematic of the combustor with different fuel injection strut arrangements is given in Fig. 1. Two types of fuel injection struts are explored in the numerical simulations: The first one is a five-faced diamond-shaped strut connected to the top and bottom walls with a small leading-edge angle to keep the shock attached. The trailing edge is kept blunt for flame-holding purposes. A swept-back configuration with an obtuse total angle is considered as the second type of strut. The Marquardt Corporation has investigated this type of strut in a scramjet combustor to increase the three-dimensionality of the flow. Like the diamond-shaped strut, sharp leading edges and blunt trailing edges have also been provided to keep this shock attached and to keep its flame-holding purpose, respectively. In all of the simulations, there are five struts. Liquid hydrocarbon is injected from a number of injection holes from the struts, top wall, and side walls. Fuel is also injected downstream of the backward-facing step

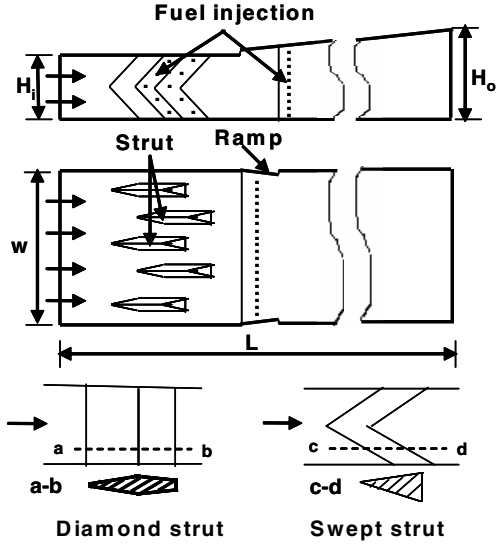

Fig. 1 Schematic sketch of the scramjet combustor with various strut arrangements.

Table 1 Combustor geometrical dimensions and inlet boundary conditions

	Case 1	Case 2	Case 3	Case 4
Length, L/W	6.74	6.74	7.37	8.04
Inlet height, H_i/W	0.37	0.41	0.41	0.28
Outlet height, H_o/W	0.84	1.06	1.13	1.09
Inlet static pressure, P_s/P_α	65.5	43.7	43.7	65.5
Inlet total pressure, P_o/P_α	597.2	726.0	726.0	1080.8
Inlet static temperature, T_s/T_α	5.18	4.48	4.48	4.48
Inlet total temperate, T_o/T_α	8.17	8.17	8.17	8.17
Inlet Mach number	2.0	2.5	2.5	2.5
Inlet mass flow, kg/s	4.25	4.25	4.25	4.25
Fuel injection equivalence ratio, ϕ	1.0	1.0	1.0	1.0
Strut	0.50	0.58	0.64	0.57
Top wall	0.20	0.21	0.18	0.23
Side wall	0.30	0.21	0.18	0.20
Inlet air composition				
O_2	0.23	0.23	0.23	0.23
H_2O	0.18	0.18	0.18	0.18
N_2	0.59	0.59	0.59	0.59

from the top wall and from the ramps of the side wall. The injection holes have a diameter of 0.4 mm and 290 g/s fuel is injected in the combustor. The dimensions of the combustor, fuel equivalence ratios injected from the top and side walls and the struts, and the vitiated-air compositions are given in Table 1. All of the lengths are nondimensionalized with the width W of the half-module combustor, and the pressures and temperatures are nondimensionalized with their freestream values.

III. Methodology

The software used in the present study is the three-dimensional Navier–Stokes code CFX-TASCflow, which is an integrated software system capable of solving diverse and complex multidimensional fluid-flow problems. The code is a fully implicit finite volume method with finite-element-based discretization of geometry. The method retains much of the geometric flexibility of finite element methods, as well as the important conservation properties of the finite volume method. It uses numerical upwind schemes to ensure global convergence of mass, momentum, energy, and species. It implements general nonorthogonal, structured, boundary-fitted grids. In the present study, to circumvent the initial numerical transient, the discretization of the convective terms are done by a first-order upwind-difference scheme for a few time steps and then the convective terms are discretized through a second-order scheme to capture the flow features more accurately. The turbulence model used is K-ε model with wall functions. To investigate the accuracy and the range of applications, the software is validated for various reacting and nonreacting flows pertaining to the scramjet combustor, including transverse sonic injection in supersonic flow [31], transverse H_2 injection in a constant-area duct [32], and staged H_2 injection from the struts [33] and pylon injectors [34]. All of these validation exercises revealed that although the computed pressures overpredict the experimental values in the injection zone, the computational and experimental values of the flow parameters match fairly well in the divergent portion of the combustor in which the major portion of thrust is produced.

A. Governing Equations

The appropriate system of equations governing the turbulent flow of a compressible gas may be written as follows:

Continuity equation:

$$\frac{\partial \rho}{\partial t} + \frac{\partial}{\partial x_k}(\rho u_k) = 0 \qquad k = 1, 2, 3$$

Momentum equation:

$$\frac{\partial}{\partial t}(\rho u_i) + \frac{\partial}{\partial x_k}(\rho u_i u_k) + \frac{\partial P}{\partial x_i} = \frac{\partial(\tau_{ik})}{\partial x_k}, \qquad i, k = 1, 2, 3$$

Energy equation:

$$\frac{\partial}{\partial t}(\rho H) + \frac{\partial}{\partial x_k}(\rho u_k H) = -\frac{\partial}{\partial x_k}(u_j \tau_{jk}) + \frac{\partial q_k}{\partial x_k} \qquad j, k = 1, 2, 3$$

Turbulent kinetic energy K equation:

$$\frac{\partial}{\partial t}(\rho K) + \frac{\partial}{\partial x_k}(\rho u_k K) = \frac{\partial}{\partial x_k}\left(\left(\frac{\mu_l}{Pr} + \frac{\mu_t}{\sigma_K}\right)\frac{\partial K}{\partial x_k}\right) + S_K$$

Rate of dissipation of turbulent kinetic energy ε equation:

$$\frac{\partial}{\partial t}(\rho \varepsilon) + \frac{\partial}{\partial x_k}(\rho u_k \varepsilon) = \frac{\partial}{\partial x_k}\left(\left(\frac{\mu_l}{Pr} + \frac{\mu_t}{\sigma_\varepsilon}\right)\frac{\partial \varepsilon}{\partial x_k}\right) + S_\varepsilon$$

Species mass fraction Z:

$$\frac{\partial}{\partial t}(\rho Z) + \frac{\partial}{\partial x_k}(\rho u_k Z) = \frac{\partial}{\partial x_k}\left(\left(\frac{\mu_l}{Pr} + \frac{\mu_t}{\sigma_c}\right)\frac{\partial Z}{\partial x_k}\right)$$

where ρ, u_i, p, and H are the density, velocity components, pressure, and total energy, respectively; $\mu = \mu_l + \mu_t$ is the total viscosity (with μ_l and μ_t being the laminar and turbulent viscosities); Pr is the Prandtl number; and the source terms S_k and S_ε of the K and ε equation are defined as

$$S_K = \tau_{ik}\frac{\partial u_i}{\partial x_k} - \rho\varepsilon \quad \text{and} \quad S_\varepsilon = C_{\varepsilon 1}\tau_{ik}\frac{\partial u_i}{\partial x_k} - C_{\varepsilon 2}\frac{\rho\varepsilon^2}{K}$$

where turbulent shear stress is defined as

$$\tau_{ik} = \mu_t\left(\frac{\partial u_i}{\partial x_k} + \frac{\partial u_k}{\partial x_i}\right)$$

Laminar viscosity μ_l is calculated from the Sutherland law as

$$\mu_l = \mu_{\text{ref}}\left(\frac{T}{T_{\text{ref}}}\right)^{3/2}\left(\frac{T_{\text{ref}} + S}{T + S}\right)$$

where T is the temperature and μ_{ref}, T_{ref}, and S are known values. The turbulent viscosity μ_t is calculated as

$$\mu_t = c_\mu \frac{\rho K^2}{\varepsilon}$$

The coefficients involved in the calculation of μ_t are taken as

$$c_\mu = 0.09, \qquad C_{\varepsilon 1} = 1.44, \qquad C_{\varepsilon 2} = 1.92$$
$$\sigma_K = 1.0, \qquad \sigma_\varepsilon = 1.3, \qquad \sigma_c = 0.9$$

The heat flux q_k is calculated as $q_k = -\lambda(\partial T/\partial x_k)$, where λ is the coefficient of thermal conductivity.

B. Combustion Modeling

For combustion, the eddy-dissipation model (EDM) is used for its simplicity and robust performance in predicting reactive flows. The EDM is based on the concept that chemical reaction is fast relative to the transport process in the flow. When reactants mix at the molecular level, they instantaneously form products. The model assumes that the reaction rate may be related directly to the time required to mix reactants at the molecular level. In turbulent flows, this mixing time is dictated by the eddy properties, and therefore the burning rate is proportional to the rate at which turbulent kinetic energy is dissipated; that is, the reaction rate is proportional to ε/K, where K is the turbulent kinetic energy and ε is its rate of dissipation. The chemistry of the combustion reaction is represented on a molar basis by

$$C_{12}H_{23} + 17.75O_2 = 12CO_2 + 11.5H_2O$$

The mixing rate determined from the EDM is given as

$$R_{k,\mathrm{EDM}} = -A_{\mathrm{ebu}}\rho\frac{\varepsilon}{K}\min\left\{Y_f, \frac{Y_o}{r_k}, B_{\mathrm{ebu}}\frac{Y_p}{1+r_k}\right\}$$

where ρ is the density; Y_f, Y_o, and Y_p are the mass fractions of the fuel, oxidizer, and products, respectively; A_{ebu} and B_{ebu} are the model constants; and r_k is the stoichiometric ratio.

C. Discrete-Phase Model

Lagrangian tracking method is used for the discrete-phase model to characterize the flow behavior of the dispersed-phase fluid (kerosene liquid). The prediction of flows involving the dispersed phase involves the separate calculation of each phase with source terms generated to account for the interaction between the phases. The flow of the continuous phase is predicted using a discretized form of the Navier–Stokes equations. There is no continuum with the dispersed phase, and each particle interacts with the fluid and other particles discretely. Therefore, the most widely applied method available to determine the behavior of the dispersed phase is to track several individual particles through the flowfield. Each particle represents a sample of particles that follow an identical path. The behavior of the tracked particles is used to describe the average behavior of the dispersed phase. Only viscous drag on the particles is considered in the study. Particle–particle interactions and the effect of turbulence in the discrete phase are not simulated in the analysis.

D. Source Terms for Governing Equations

For the purpose of describing the types of sources generated by particles, it is convenient to consider the differences between inert and reacting particles. Both inert and reacting components of particles exchange momentum with the fluid, due to viscous drag and exchange energy due to particle heating. Reacting particles may also exchange mass with the fluid, as well as exchange momentum and energy due to mass sources. If the sources are grouped according to inert components (those sources common to all particle types) and reacting components (those sources only found with reacting particles), then particle sources may be generalized as shown in Table 2. The details of the formulation are available in [29].

E. Discretization of Governing Equations

The CFX-TASCflow solver uses a finite volume approach in which the conservation equations in differential form are integrated over a control volume described around a node, to obtain an integral equation. The pressure integral terms in the momentum integral equation and the spatial derivative terms in the integral equations are evaluated using a finite element approach. An element is described with eight neighboring nodes. The advective term is evaluated using upwind differencing with physical advection correction. The set of discretised equations form a set of algebraic equations: $A\boldsymbol{x} = b$, where $\boldsymbol{x}$ is the solution vector. The solver uses an iterative procedure to update an approximated x_n (solution of x at the nth time level) by solving for an approximate correction x' from the equation $A\boldsymbol{x}' = \boldsymbol{R}$, where $\boldsymbol{R} = \boldsymbol{b} - A\boldsymbol{x}_n$ is the residual at the nth time level. The equation $A\boldsymbol{x}' = \boldsymbol{R}$ is solved approximately using an approach called the incomplete lower/upper factorization method. An algebraic multigrid method is implemented to reduce low-frequency errors in the solution of the algebraic equations. Maximum residual

Table 2 Particle source terms

Source	Inert component	Reacting component
Mass	——	$\dot{N}\delta m_p$
Momentum	$\dot{N}m_p(v_p - v_f)$ $[1-\exp(-18\mu\delta t/\rho d^2)]$	$\dot{N}\delta m_p v_p$
Energy	$\dot{N}\int_0^{\delta t} h_c A_p(T_f - T_p)\,\mathrm{d}t$	$\dot{N}(-L_v\delta m_v + Q_c\delta m_c)$

$$\left(\phi_j^{n+1} - f\left(\phi_j^{n+1}, \phi_j^n\right)\right) < 10^{-4}$$

is taken as the convergence criteria.

IV. Results and Discussion

Taking advantage of the geometrical symmetry, only one-half of the combustor is considered as the computational domain. The grid is fine near the struts, near-wall region, backward-facing step, and adjacent to the ramp zone; the relatively coarse grid is provided in the remaining portion of the combustor. In the simulation, the X axis is taken along the length of the combustor, and the Y and Z axes are chosen along the width and the height of the combustor. The origin is placed at the inlet of the combustor at the middle of the bottom surface. Because the injection holes are very small in diameter ($\sim$0.4 mm), the original grids are made finer by doing the grid embedment adjacent to each injection point. The grid embedment has approximated the circular hole as the rectangular hole with the same equivalent area. Because the area of the hole is very small, this approximation is not likely to effect the flow development.

All the flow properties are kept constant in the inflow plane, because the inflow boundary is supersonic. Solid-wall and adiabatic-wall boundary conditions are applied on the wall and a supersonic outflow boundary condition is applied at the exit of the computational domain. Symmetric condition is applied in the plane of symmetry. A log-normalized residue of 10^{-4} is considered as the convergence criteria.

Mach number distributions at various cross-sectional planes at $X/L = 0.0$, 0.2, 0.4, 0.6, 0.8, and 1.0 (L is the length of the combustor) for the geometries with diamond-shaped (case 1) and swept struts (case 3) are presented in Figs. 2 and 3 to depict the flow development process inside the combustor. Because of shock from the fuel injection strut and heat release, the Mach number is seen to reduce downstream of the strut and to again accelerate due to divergence of the combustor. Although the Mach number reduces significantly due to heat addition and few subsonic pockets are there, normal shock did not appear. Axial distributions of the area-averaged Mach number between the four cases are compared in Fig. 4. For case 1, the area-averaged Mach number is less than unity in the region $X/W = 0.9$–2.0, whereas it is more than unity for the other three cases. The axial variations of the subsonic region for all of the cases are compared in Fig. 5. For case 1, due to a comparatively lower combustor-entry Mach number and intense heat release in the constant-area portion, nearly 80% of the area is subsonic between $X/W = 0.5$–2.5. For other cases, the subsonic area is much smaller, mainly due to a higher inlet Mach number and the distributed-fuel-injection pattern. The axial variations of nondimensionalized surface pressure at the top wall at the symmetry plane for reacting and nonreacting flows are compared in Fig. 6 for case 1. The pressure is

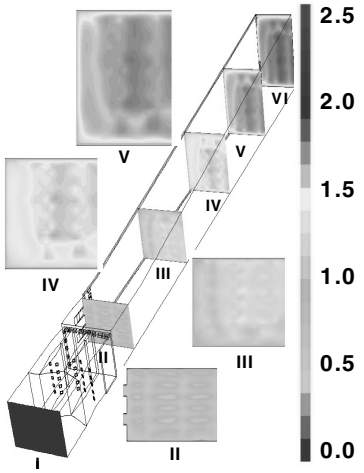

Fig. 2 Mach number distribution for case 1; X/L values are 0 (I), 0.2 (II), 0.4 (III), 0.6 (IV), 0.8 (V), and 1.0 (VI).

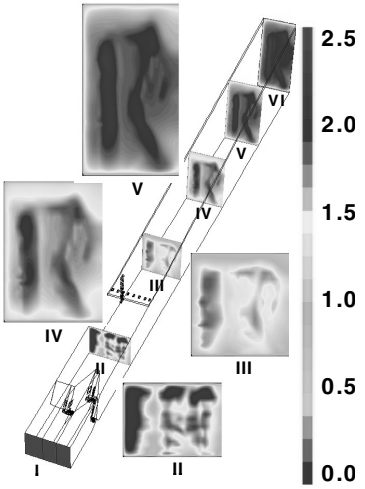

Fig. 3 Mach number distribution for case 3; X/L values are 0 (I), 0.2 (II), 0.4 (III), 0.6 (IV), 0.8 (V), and 1.0 (VI).

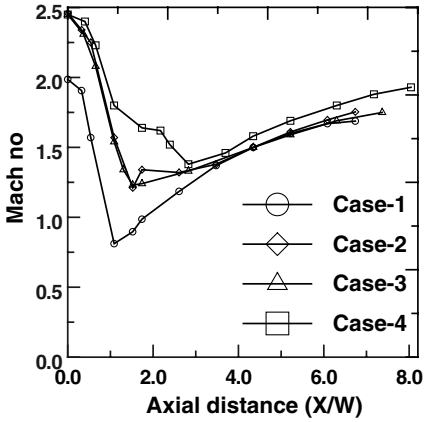

Fig. 4 Comparison of the axial variation of the area-averaged Mach number.

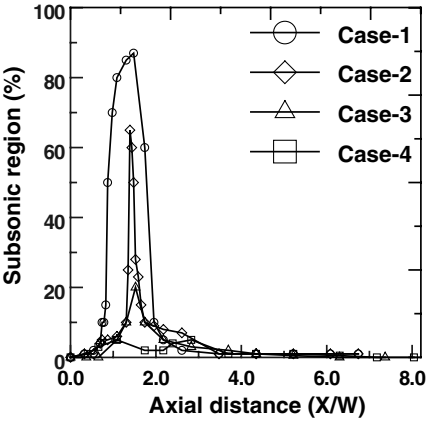

Fig. 5 Comparison of the subsonic region.

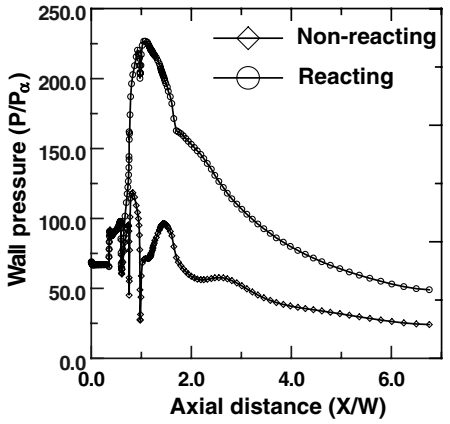

Fig. 6 Comparison of reacting and nonreacting surface pressures for case 1.

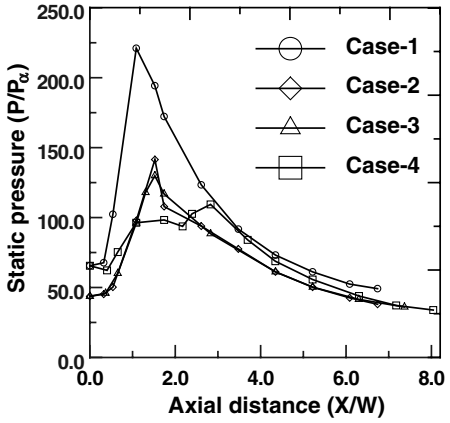

Fig. 7 Comparison of static pressure.

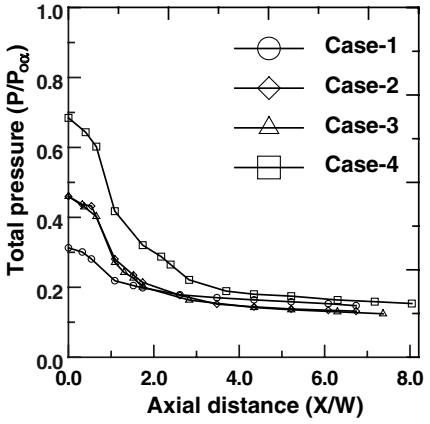

Fig. 8 Comparison of the area-averaged total pressure.

normalized with the freestream pressure at 32.5-km altitude. The pressure is uniform until the oblique shock from the leading edge of the strut hit the combustor wall. The pressure is seen to decrease due to flow expansion behind the downstream of the strut. Few shock reflections are seen in the nonreacting cases. Kerosene combustion has increased the pressure very significantly for the reacting case, and significant differences in surface pressure between the reacting and nonreacting cases are seen throughout the combustor. The area-averaged nondimensionalized static pressure distribution in all four cases is compared in Fig. 7. The static pressure for case 1 is seen to be significantly higher for case 1 than with the other cases, due to high heat release in the constant-area portion. The area-averaged nondimensionalized total pressure distribution is compared for all four cases in Fig. 8. The higher the total pressure at entry, the greater the loss in total pressure.

The axial distribution of area-averaged temperature and heat-release values are compared for the four cases in Figs. 9 and 10, respectively. The maximum difference of the temperature between these four cases is on the order of 200 K. The heat-release rate for

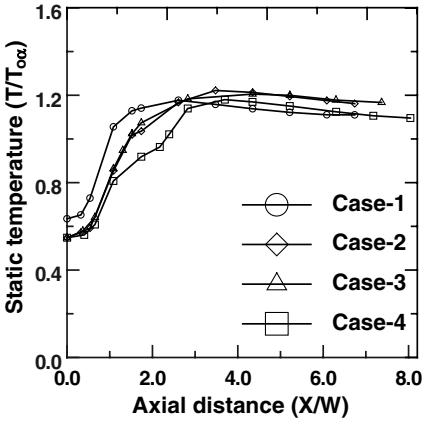

Fig. 9 Comparison of the static temperature distribution.

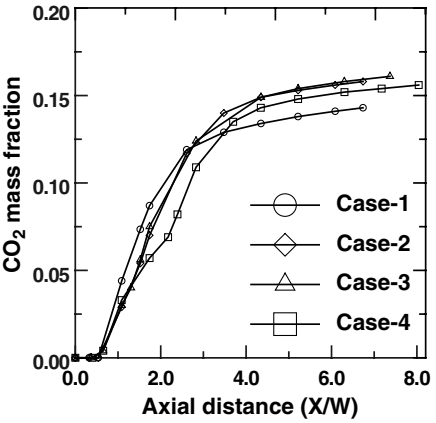

Fig. 12 Comparison of CO_2 distribution.

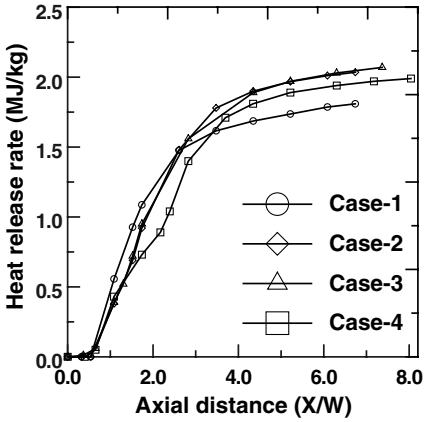

Fig. 10 Comparison of the heat-release rate.

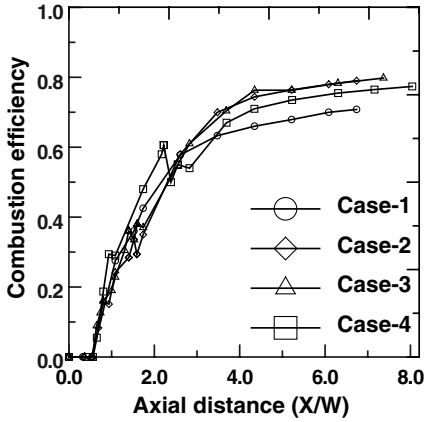

Fig. 13 Comparison of combustion efficiency.

case 1 is sharper, whereas the heat-release rate for case 4 is more gradual. This is because the injection pattern is more distributed in case 4 than in case 1. It is to be noted that the computed heat release will be higher in the injection zone because of the infinitely fast chemistry assumption. This may lead to a lower Mach number in the injection zone. But in the design studies, we have to ensure the predominant supersonic region throughout the combustor through proper tailoring of heat release.

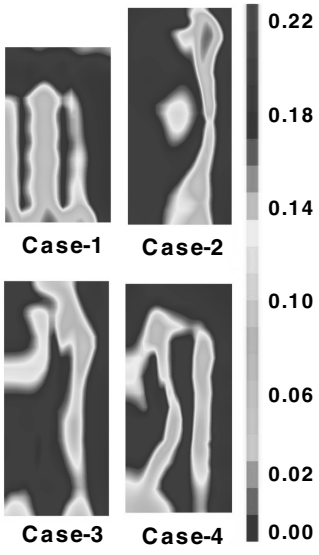

Fig. 11 CO_2 distribution at the exit of the combustor.

The cross-sectional views of CO_2 mass fractions at combustor exit planes for the four cases are compared in Fig. 11. Although a large amount of CO_2 is seen to present at the exit sections of the combustors, some patches of not-so-intensive reaction zones are still present at these exit sections. This is due to nonmixing of fuel and oxidizer in the combustor. The axial distribution of area-averaged CO_2 mass fraction is shown in Fig. 12. The rate of CO_2 formation for case 1 has become slower at $X/W = 3$, whereas for the other cases, the CO_2 formation is showing an increasing trend. The axial variations of the combustion efficiencies for all of the cases are compared in Fig. 13. The combustion efficiency is defined as the ratio of the actual CO_2 formed to the ideal CO_2 that can be formed from the reaction. The combustion efficiencies at the exit of the combustor are seen to vary in the range of 71 to 81%. The calculated thrust and the combustion efficiencies of the four cases are compared in Table 3.

A significant amount of thrust is obtained for case 1 in spite of having minimum combustion efficiencies. It indicates that the incurred drag due to fuel injection struts and other protrusions in the flowpath for the other three cases are higher than for case 1.

To investigate the effect of three-dimensionality in the flowfield, the top, bottom, and side-wall surface pressures are compared in Fig. 14 for these different cases. For case 1, because the struts are

Table 3 Comparison of thrust and combustion efficiencies for the four cases

Cases	Combustion efficiency	Thrust, N
1	71	1736
2	79	1452
3	81	1609
4	78	1785

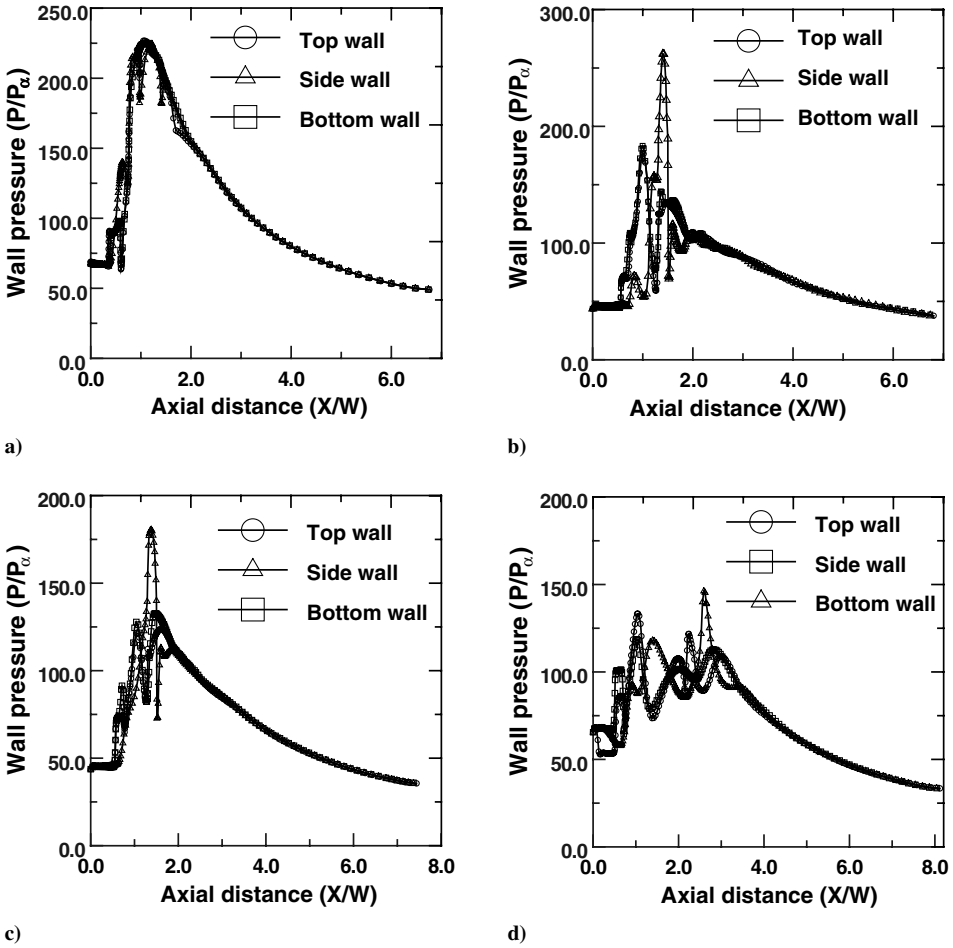

Fig. 14 Comparison of wall pressure distribution for a) case 1, b) case 2, c) case 3, and d) case 4.

regular in shape, the variation of pressure between the top and side walls is seen up to $X/W = 1.8$, and beyond that, almost all of the values are merged into a single curve. For other cases, there are significant differences of the surface pressure between the three walls up to $X/W = 3.5$. It can be recalled that for cases 2, 3, and 4, swept struts are used to increase the three-dimensionality of the flowfield. This demonstrate the necessity of doing a three-dimensional simulation to predict the flowfield in a scramjet combustor.

V. Conclusions

Numerical simulations are carried out to analyze the flowfield of a strut-based liquid-kerosene-fueled scramjet combustor. Commercial CFD software CFX-TASCflow is used to solve three-dimensional Navier–Stokes equations, along with a K-ε turbulence model. Combustion is modeled by the eddy-dissipation concept based on infinitely fast rate kinetics. The evaporation and mixing of liquid-kerosene droplets is studied by employing a Lagrangian dispersed-phase analysis. The performance of two different kinds of struts (namely, five-faced diamond struts and swept-back struts) are studied to predict the flow development process in the scramjet combustor. The thermochemical behavior of various flow parameters is analyzed through comparison of cross-sectional views at different longitudinal locations and the axial distribution of area-averaged properties. The computed heat release in the injection zone is higher because of fast chemistry assumption, which may lead to lowering of the Mach number in the injection zone. A higher inlet Mach number and a distributed-fuel-injection system are required to ensure a predominant supersonic flow throughout the combustor. Parametric studies are also carried out to investigate the effect of combustor-entry Mach number and total pressure in the flowfield. The comparisons of computed thrust and combustion efficiency between the cases revealed that higher combustion efficiency does not necessarily lead to higher thrust; the drag incurred by the fuel injection struts also plays a significant role in determining the scramjet combustor performance. The comparisons of surface pressure at different walls demonstrate that the distributed injection system increases the three-dimensional flowfield, and it is necessary to do a three-dimensional calculation for the realistic prediction of scramjet combustor performance.

References

[1] Northam, G. B., and Anderson, G. Y., "Supersonic Combustion Ramjet Research at Langley," AIAA Paper 86-0159, 1986.

[2] Waltrup, P. J., "Liquid–Fueled Supersonic Combustion Ramjet: A Research Perspective," *Journal of Propulsion and Power*, Vol. 3, No. 6, 1987, pp. 515–524.

[3] Kush, E. A., and Schetz, J. A., "Liquid Jet Injection into a Supersonic Flow," *AIAA Journal*, Vol. 11, No. 9, 1973, pp. 1223–1224.

[4] Abbitt, J. D., III., Hartfiled, R. J., and McDaniel, J. C., "Mole-Fraction Imaging of Transverse Injection in a Ducted Supersonic Flow," *AIAA Journal*, Vol. 29, No. 3, 1991, pp. 431–435.

[5] Yokota, K., and Kaji, S., "Two- and Three-Dimensional Study on Supersonic Flow and Mixing Fields with Hydrogen Injection," AIAA Paper 95-6024, 1995.

[6] Miyajima, H., Chinzei, N., Mitani, T., Wakamatser, Y., and Maita, M., "Development Status of the NAL Ramjet Engine Test Facility and Subscale Scramjet Engine," AIAA Paper 92-5094, 1992.

[7] Sunami, T., Sakuranaka, N., Tani, K., Kiraiwa, T., and Shimura, T., "Mach 4 Test of a Scramjet Engine–Effect of Isolator," *Proceeding of 13th International Symposium of Air-Breathing Engine*, AIAA, Washington, D.C., 1997, pp. 615–625.

[8] Kanda, T., Hiraiwa, T., Mitani, T., Tomioka, S., and Chinzei, N., "Mach 6 Testing of a Scramjet Engine Model," *Journal of Propulsion and Power*, Vol. 13, No. 4, 1997, pp. 543–551.

[9] Kanda, T., Sunami, T., Tomioka, S., Tani, K., and Mitani, T., "Mach 8 Testing of Scramjet Engine Model," *Journal of Propulsion and Power*,

Vol. 17, No. 1, 2001, pp. 132–138.
[10] Masuya, G., Komuro, T., Murakami, A., Shinozaki, N., Nakamura, A., Murayama, M., and Ohwaki, K., "Ignition and Combustion Performance of Scramjet Combustors with Fuel Injection Struts," *Journal of Propulsion and Power*, Vol. 11, No. 2, 1995, pp. 301–307.
[11] Mitani, T., Kanda, T., Hiraiwa, T., Igarashi, Y., and Nakahashi, K., "Drags in Scramjet Engine Testing: Experimental and Computational Fluid Dynamics Studies," *Journal of Propulsion and Power*, Vol. 15, No. 4, 1999, pp. 578–583.
[12] Mitani, T., Chinzei, N., and Kanda, T., "Reaction and Mixing-Controlled Combustion in Scramjet Engines," *Journal of Propulsion and Power*, Vol. 17, No. 2, 2001, pp. 308–314.
[13] Gerlinger, P., Kasal, P., Stoll, P., and Bruggemann, D., "Experimental and Theoretical Investigation on 2D and 3D Parallel Hydrogen/Air Mixing in a Supersonic Flow," ISABE Paper 2001-1019, 2001.
[14] Tomioka, S., Murakami, A., Kudo, K., and Mitani, T., "Combustion Tests of a Staged Supersonic Combustor with a Strut," *Journal of Propulsion and Power*, Vol. 17, No. 2, 2001, pp. 293–300.
[15] Tomioka, S., Kobayashi, K., Kudo, K., Murakami, A., and Mitani, T., "Effects of Injection Configuration on Performance of a Staged Supersonic Combustor," *Journal of Propulsion and Power*, Vol. 19, No. 5, 2003, pp. 876–884.
[16] Glawe, D. D., Saminy, M., Nejad, A. S., and Cheng, T. H., "Effects of Nozzle Geometry on Parallel Injection from Base of an Extended Strut into a Supersonic Flow," AIAA Paper 95-0522, 1995.
[17] Wepler, U., and Koschel, W., "Numerical Investigation of Turbulent Reacting Flows in a Scramjet Combustor Model," AIAA Paper 2002-3572, 2002.
[18] Mathur, T., Gruber, M., Jackson, K., Donbar, J., Donaldson, W., Jackson, T., and Billig, F., "Supersonic Combustion Experiments with a Cavity-Based Fuel Injector," *Journal of Propulsion and Power*, Vol. 17, No. 6, 2001, pp. 1305–1312.
[19] Li, J. G., Yu, G., Zhang, X. Y., and Huang, Q. S., "Combustion of Kerosene in a Supersonic Stream," AIAA Paper 2000-0615, 2000.
[20] Burnes, R., Parr, T. P., Wilson, K. J., and Yu, K., "Investigation of Supersonic Mixing Control Using Cavities–Effect of Fuel Injection Location," AIAA Paper 2000-3618, 2000.
[21] Yu, K. H., Wilson, K. J., and Schadow, K. C., "Effect of Flame Holding Cavities on Supersonic—Combustion Performance," *Journal of Propulsion and Power*, Vol. 17, No. 6, 2001, pp. 1287–1295.
[22] Hsu, K. Y., Carter, C., Crafton, J., Gruber, M., Donbar, J., Mathur, T., Schommer, D., and Terry, W., "Fuel Distribution about a Cavity Flameholder in Supersonic Flow," AIAA Paper 2000-3585, 2000.
[23] Gruber, M. R., Donbar, J. M., Carter, C. D., and Hsu, K. Y., "Mixing and Combustion Studies Using Cavity-Based Flameholders in a Supersonic Flow," *Journal of Propulsion and Power*, Vol. 20, No. 5, 2004, pp. 769–778.
[24] Yu, G., Li, J. G., Chang, X. Y., Chen, L. H., and Sung, C. J., "Fuel Injection and Flame Stabilization in a Liquid–Kerosene Fueled Supersonic Combustor," *Journal of Propulsion and Power*, Vol. 19, No. 5, 2003, pp. 885–893.
[25] Vinogradov, V. A., Kobigsky, S. A., and Petrov, M. D., "Experimental Investigation of Kerosene Fuel Combustion in Supersonic Flow," *Journal of Propulsion and Power*, Vol. 11, No. 1, 1995, pp. 130–134.
[26] Bouchez, M., Dufour, E., and Montazel, X., "Hydrocarbon Fueled Scramjet for Hypersonic Vehicles," AIAA Paper 1998-1589, 1998.
[27] Dufour, E., and Bouchez, M., "Computational Analysis of a Kerosene-Fueled Scramjet," AIAA Paper 2001-1817, 2001.
[28] Behera, R., and Chakraborty, D., "Numerical Simulation of Combustion in Kerosene Fueled Ramp Cavity Based Scramjet Combustor," *Journal of Aerospace Sciences and Technologies*, Vol. 58, No. 2, 2006, pp. 104–111.
[29] CFX-TASCflow, Software Package, Ver. 2.11.1, AEA Technology Engineering Services, Inc., Mooresville, NC, 2001.
[30] Panneerselvam, S., Thiagarajan, V., Ganesh, A. T. K., Geetha, J. J., Ramanujachari, V., and Prahlada, "Airframe Integrated Scramjet Design and Performance Analysis," International Symposium on Air Breathing Engines Paper 2005-1280, 2005.
[31] Manna, P., and Chakraborty, D., "Numerical Investigation of Transverse Sonic Injection in a Nonreacting Supersonic Combustor," *Proceedings of the Institution of Mechanical Engineers, Part G (Journal of Aerospace Engineering)*, Vol. 219, No. 3, 2005, pp. 205–215.
doi:10.1243/095441005X30261
[32] Manna, P., and Chakraborty, D., "Numerical Simulation of Transverse H_2 Combustion in Supersonic Airstream in a Constant Area Duct," *Journal of the Institution of Engineers (India)*, Vol. 86, Nov. 2005, pp. 47–53.
[33] Saha, S., and Chakraborty, D., "Reacting Flow Computation of Staged Supersonic Combustor with Strut Injection," AIAA Paper 2006-3895, 2006.
[34] Javed, A., and Chakraborty, D., "Numerical Simulation of Supersonic Combustion of Pylon Injected Hydrogen Fuel in Scramjet Combustor," *Journal of the Institution of Engineers (India)*, Vol. 87, May 2006, pp. 1–6.

J. Oefelein
Associate Editor